Surface chemistry and bonding configuration of ultrananocrystalline diamond surfaces and their effects on nanotribological properties

A. V. Sumant,[1,*] D. S. Grierson,[1] J. E. Gerbi,[2,†] J. A. Carlisle,[2,3,‡] O. Auciello,[2,3] and R. W. Carpick[1,§]
[1]*Department of Engineering Physics, University of Wisconsin–Madison, Wisconsin 53706, USA*
[2]*Materials Science Division, Argonne National Laboratory, Argonne, Illinois 60439, USA*
[3]*Center for Nanoscale Materials, Argonne National Laboratory, Argonne, Illinois 60439, USA*
(Received 2 March 2007; revised manuscript received 13 August 2007; published 26 December 2007)

We present a comprehensive study of surface composition and nanotribology for ultrananocrystalline diamond (UNCD) surfaces, including the influence of film nucleation on these properties. We describe a methodology to characterize the underside of the films as revealed by sacrificial etching of the underlying substrate. This enables the study of the morphology and composition resulting from the nucleation and initial growth of the films, as well as the characterization of nanotribological properties which are relevant for applications including micro-/nanoelectromechanical systems. We study the surface chemistry, bonding configuration, and nanotribological properties of both the topside and the underside of the film with synchrotron-based x-ray absorption near-edge structure spectroscopy to identify the bonding state of the carbon atoms, x-ray photoelectron spectroscopy to determine the surface chemical composition, Auger electron spectroscopy to further verify the composition and bonding configuration, and quantitative atomic force microscopy to study the nanoscale topography and nanotribological properties. The films were grown on SiO_2 after mechanically polishing the surface with detonation synthesized nanodiamond powder, followed by ultrasonication in a methanol solution containing additional nanodiamond powder. The sp^2 fraction, morphology, and chemistry of the as-etched underside are distinct from the topside, exhibiting a higher sp^2 fraction, some oxidized carbon, and a smoother morphology. The nanoscale single-asperity work of adhesion between a diamond nanotip and the as-etched UNCD underside is far lower than for a silicon-silicon interface (59.2 ± 2 vs 826 ± 186 mJ/m^2, respectively). Exposure to atomic hydrogen dramatically reduces nanoscale adhesion to 10.2 ± 0.4 mJ/m^2, at the level of van der Waals' interactions and consistent with recent *ab initio* calculations. Friction is substantially reduced as well, demonstrating a direct link between the surface chemistry and nanoscale friction. The proposed mechanism, supported by the detailed surface spectroscopic analysis, is the elimination of reactive (e.g., C*—), polar (e.g., C═O), and π-bonded (C═C) surface groups, which are replaced by fully saturated, hydrogen-terminated surface bonds to produce an inert surface that interacts minimally with the contacting counterface.

DOI: 10.1103/PhysRevB.76.235429 PACS number(s): 61.10.Ht, 82.65.+r, 68.35.Af, 81.05.Uw

I. INTRODUCTION

Understanding the composition and bonding of materials at or near surfaces is a fundamental scientific and technological need that cuts across many disciplines. It is particularly important for interfaces in contact, where adhesion, friction, and tribochemical reactions are influenced or controlled by the composition and bonding state of the contacting surfaces. At the nanoscale, the dominance of the surface over the bulk renders such considerations essential for implementing reliable micro- and nanoelectromechanical systems (MEMS/NEMS), for example, which involve interfaces in mechanical contact.

The extraordinary mechanical and tribological properties of diamond[1] make it not only of significant continued interest scientifically but also render it a tantalizing candidate as a structural material for MEMS/NEMS. However, fabricating MEMS/NEMS devices with conventional microcrystalline diamond, grown by chemical vapor deposition (CVD), is a challenging task because of the large grain size (1–5 μm in diameter), high roughness (usually 10% of the film thickness), and high internal stress (a few gigapascals). Recently, nanocrystalline diamond (NCD) films,[2] with grain sizes below 50 nm, and ultrananocrystalline diamond (UNCD) films,[3] with grain sizes below 10 nm, have shown promise to overcome these barriers. Several groups have conducted extensive studies on diamond as a MEMS/NEMS material.[4–7]

UNCD, the focus of this work, has phase-pure diamond grains and atomically abrupt grain boundaries, with up to 95%–98% sp^3 bonding overall. Synthesized using a hydrogen-poor Ar/CH_4 gas chemistry, it has grain sizes in the range of 2–10 nm and possesses very smooth surfaces (rms roughness 7–11 nm over a 10×10 μm^2 area).[3] A range of surface-micromachined MEMS structures (e.g., cantilevers and fixed-fixed beams) was fabricated from UNCD,[8] and measurements of its mechanical properties confirm its Young's modulus (980 GPa),[9,10] hardness (95 GPa),[9] and fracture toughness (4.5 ± 0.25 MPa m$^{1/2}$)[11] are in the range of single crystal diamond. Recent measurements of the work of adhesion and friction forces between tungsten carbide (WC) tips and UNCD surfaces showed intrinsically low values which were comparable to those measured between WC and single crystal diamond surfaces.[12] These properties demonstrate the potential of UNCD as a structural material for tribologically demanding MEMS/NEMS applications.[8,9,13,14]

Studying how the chemistry and bonding configuration of UNCD surfaces affect adhesion and friction provides an op-

portunity to develop the physical basis of nanotribological interactions for a particularly interesting nanostructured material. Furthermore, this knowledge is required to study the feasibility and enables the design and fabrication of reliable, working diamond-based MEMS/NEMS devices involving tribological contact.

In this paper, we present detailed studies on the morphology, surface chemistry, bonding configuration, and nanotribology of tribologically relevant UNCD surfaces, namely, both the naturally exposed topside of the film and the underside of the film after sacrificial etching of the substrate. We demonstrate a method to control adhesion forces down to the van der Waals' limit, which also significantly reduces friction.

II. EXPERIMENT

UNCD thin films were grown on silicon substrates that had a thermally grown, ~1 μm thick SiO_2 layer. Prior to UNCD growth, the substrates were first lightly mechanically polished with detonation synthesized diamond nanopowder (commercially available, particle size ~10 nm) followed by ultrasonic agitation in a methanol solution containing additional diamond nanopowder. UNCD films were then grown on this seeded substrate in an IPLAS (Innovative Plasma Systems GmbH, Troisdorf, Germany) CYRRANUS I 6 in. reactor. The deposition parameters were 49.2 SCCM (SCCM denotes cubic centimeter per minute at STP) Ar, 0.8 SCCM CH_4, microwave power of 800–1200 W, chamber pressure of 150 mbar, substrate temperature of ~800 °C, and growth time of ~4 hrs. After growth, wafers were sectioned into ~1 cm^2 pieces for the subsequent experiments. Some of these films were released from the substrates to examine the underside of the UNCD film. To do this, the pieces were immersed in a $HF:HNO_3$ (1:3) acid bath, dissolving the Si/SiO_2 substrate and resulting in freestanding UNCD membranes. These membranes were further cleaned by rinsing in acetone, methanol, and ethanol and retrieved using a clean Si substrate, ensuring that the newly exposed underside of the UNCD film remained facing up. To hold this membrane in place, dots of silver epoxy were applied to its sides. The process sequence is illustrated in Fig. 1.

Some of these "bottom side up" membranes were subsequently treated with a hydrogen plasma in an inductively coupled 13.56 MHz RF reactor for 20 min at a pressure of 20 Torr and a temperature of ~750 °C. At the end of the process, the samples were cooled while the plasma remained on to ensure that atomic hydrogen continued to saturate dangling bonds on the UNCD surface while reducing the rate of thermally assisted desorption of hydrogen through collisions with any of the plasma species.

X-ray absorption near-edge structure (XANES) measurements were performed at the Advanced Light Source (ALS) at Lawrence Berkeley National Laboratory, Berkeley, CA. The data were acquired on beamline 8.0 which operates over the energy range from 65 to 1400 eV (at 1.5 GeV electron beam energy) using a 5 cm period undulator and a spherical-grating monochromator with three interchangeable gratings. Using 50 μm slits, the monochromator resolution was

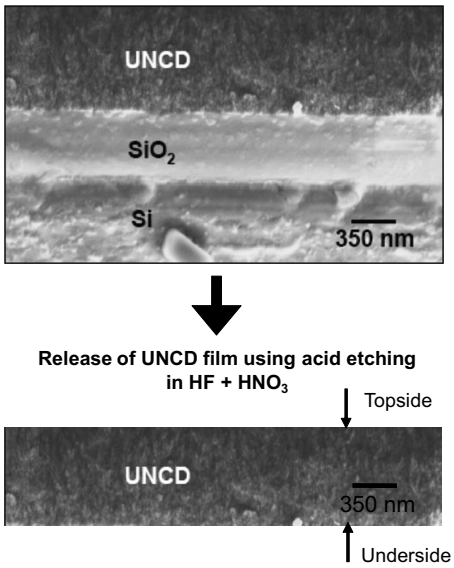

FIG. 1. Schematic illustrating the methodology used to characterize UNCD topside and underside surfaces using various spectroscopic techniques.

~0.1 eV in the region close to the carbon *K* edge. Measurements were carried out in a UHV chamber with a base pressure of 3×10^{-10} Torr. Spectra were taken in total electron yield (TEY) mode with the sample sitting at approximately normal incidence with respect to the photon beam. All spectra were normalized to the simultaneously recorded absorption current of a gold mesh positioned in the beam line to correct for the transmission structure of the monochromator and variations in the light source during the measurements. The fractions of C atoms bonded in the sp^2 configuration are determined by a peak-fitting method described in detail elsewhere.[15]

Atomic force microscopy (AFM) measurements were acquired using a Digital Instruments Nanoscope IV multimode AFM in ambient air (relative humidity recorded at ~40%) using intermittent-contact mode for imaging and contact mode for adhesion and friction measurements. Normal forces were calibrated *in situ* by the unloaded resonance method.[16] Lateral forces were calibrated using the "wedge" method.[17] Tungsten carbide cantilevers (Mikromasch, Wilsonville, OR, USA) and carbon nanotube-terminated silicon cantilevers (Vecco, Santa Barbara, CA, USA) were used for the intermittent-contact-mode images. Commercially available Si cantilevers coated with CVD diamond (Nanosensors, Neuchatel, Switzerland) were used for the adhesion and friction measurements. Shadow transmission electron microscopy (TEM) images of the diamond-coated tips were obtained using a JEOL 200 CX TEM operating at 100 keV.

X-ray photoelectron spectroscopy (XPS) measurements were obtained with a Philips PHI-5400 system with a hemispherical analyzer using a Mg anode x-ray source. Auger electron spectroscopy (AES) measurements were obtained with a Philips PHI-670 scanning Auger system with a field emission electron gun.

III. RESULTS AND DISCUSSION

A. Nucleation pretreatment and morphology control

The most widely used nucleation pretreatments for CVD diamond growth involve modification of the substrate's surface either by mechanically abrading the surface with diamond particles[18,19] or bombarding the surface with diamond particles by immersing the substrate in a diamond suspension subjected to ultrasonic agitation.[20–22] In both cases, micro- to nanoscale scratches or pits are produced on the surface, and these pits trap diamond fragments. The trapped fragments then act as nucleation sites during subsequent diamond film growth. With sufficient nucleation density, this enables the growth of a uniform, continuous diamond film. Moderate nucleation densities ranging from 10^9 to 10^{11} nuclei/cm^2 have been reported using these methods. These are roughly 7 orders of magnitude greater than that for a bare silicon surface. Abrading or mechanical polishing can cause considerable roughening of the substrate, resulting in diamond films that are not optimally smooth, and this adversely affects the optical[23] and mechanical properties of the film. The extent of the roughening depends on the manner in which the mechanical polishing is carried out. Bias-enhanced nucleation[24] is another widely used method as it does not cause any mechanical damage to the substrate. It is most effective on metallic and semiconducting substrates with the ability to form carbides since it involves implantation of carbon ions in the subsurface region, creating a carbide-rich surface that enhances diamond nucleation. However, this often results in the precipitation of a predominantly nondiamond, carbon-rich layer at the interface which, according to a recent study, is likely to have poor tribological properties.[12] The two-step process developed by Rotter[25] in 1999 and further modified by Butler and co-workers,[2,26] referred to in the literature as the "new nucleation process" (NNP), avoids most of the problems mentioned above and provides nucleation densities in excess of 10^{12} nuclei/cm^2 for the growth of NCD films on silicon.[2] Detailed spectroscopic studies[15] on the NNP revealed that the first plasma pretreatment step forms SiC along with an ultrathin layer of hydrogenated amorphous carbon on the substrate. The second ultrasonication step uniformly and densely spreads nanodiamond seed particles on this surface. This enables an extremely high nucleation density and minimizes precipitation of sp^2-bonded carbon during subsequent NCD growth enabling continuous NCD film at film thickness as low as 60 nm.

In the present case, we focus on the nucleation process involving mechanical polishing and ultrasonic seeding since this is currently the most commonly used seeding process in the literature, largely due to its convenience and reliability. We report how the surface chemistry, bonding, and morphology are affected by using this seeding process and demonstrate their relation to the tribological properties at the nanoscale.

Figures 2(a)–2(c) depict a series of scanning electron microscopy (SEM) images of UNCD films seeded using this method. The morphology of the topside (the exposed growth surface) and that of the underside (the etched nucleation side) of the UNCD surfaces [Figs. 2(a) and 2(b), respectively] are markedly different from each other. The differences are also clearly evident in the topographic AFM images [Figs. 3(a) and 3(b), respectively], where the rms roughnesses are 17.2 and 1.6 nm (measured over 5×5 μm^2 areas), respectively. The underside exhibits a uniform and extremely smooth morphology, which is expected only for an extremely high nucleation density ($>10^{11}$ nuclei/cm^2). The AFM image also reveals small polishing marks (20–60 nm wide, and several μm long, but only 1–5 nm above or below the surface), which are a result of the polishing process applied to the substrate. Isolated particles that resemble commonly observed surface debris are also seen.

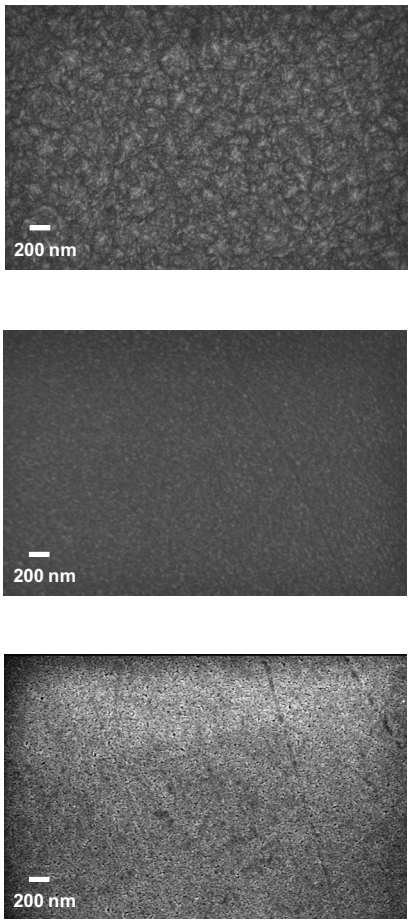

FIG. 2. [(a)–(c)] SEM images of the topside, as-etched underside, and H-terminated underside surfaces of the UNCD film.

This morphology is in striking contrast with the underside of a UNCD film seeded by a purely ultrasonic treatment without any mechanical polishing,[12] where we observed a cluster-type morphology. Each cluster consists of multiple grains and appears to have grown outward from a single initial nucleation site. The clusters are separated by narrow crevices on the underside, indicating poor nucleation density ($\sim10^8$ nuclei/cm^2). In our previous work, we referred to such UNCD clusters as "colonies."[12] Individual colonies are extremely smooth, with an rms roughness of only approximately 0.9 nm over an area of ~0.5 μm^2. The colonies exhibited a concave morphology due to time-dependent etching

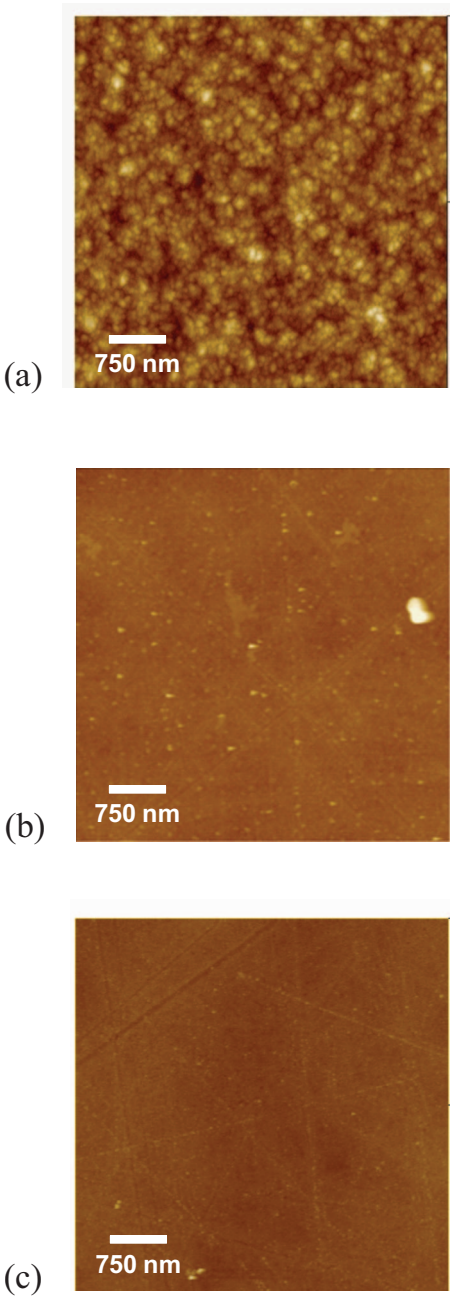

FIG. 3. (Color) [(a)–(c)] Topographic AFM images of the topside, as-etched underside, and H-terminated underside surfaces of the UNCD film.

of the oxide during growth. We have also observed this colony morphology for films grown on thermally oxidized Si samples. These results will be discussed separately.

Neither the concave morphology nor the network of colony boundaries is observed on the underside of the UNCD film seeded using the mechanical polishing with ultrasonication method [Figs. 2(b) and 3(b)]. Therefore, this nucleation method enables a substantial increase in the initial nucleation density compared with pure ultrasonication. Film coalescence presumably occurs far more rapidly because of this, and the total induction time for coalescence is therefore greatly reduced. This prevents the formation of crevices or concave morphologies that occur when the initial nucleation density is lower.

The higher nucleation density observed in this case is due to an increased density of diamond seed particles on the surface and/or the creation of a larger number of nucleation sites due to the mechanical polishing. An increased density of diamond seeds may result from the somewhat rougher morphology of the surface due to the polishing, thus trapping more seeds during ultrasonication. It may also result from an increased propensity of the diamond seeds to bond to reactive sites on the polished surface due to attractive forces. It is also possible that the polishing marks themselves present preferred nucleation sites due to increased reactivity of damaged regions of the oxide. This latter concept is supported by the observation of the transferred polishing marks in the morphology of the underside of the film [Figs. 2(b) and 3(b)].

The hydrogen plasma treatment of the UNCD underside surface [Fig. 3(c)] etches the small particles seen in Fig. 3(b) and the surface becomes smoother (rms roughness of 1.2 nm over the 5×5 μm^2 area) than before the H-plasma treatment (RMS roughness of 1.6 nm). Exposure to atomic hydrogen, either through plasma or hot-filament sources, is known to etch nondiamond phases (e.g., graphite, amorphous carbon, C—O, etc.) much more rapidly (~50 times for graphite) than pure diamond.[27] This indicates that the particles in Fig. 3(b) are nondiamond contaminants.

Much larger changes from atomic hydrogen exposure are observed on the underside of the UNCD film seeded with ultrasonic nucleation only either on silicon oxide or silicon.[12] The crevice morphology described above is correlated with a much higher concentration of sp^2-bonded carbon on the underside. The formation of this nondiamond carbon may occur because the carbon growth species become kinetically constrained within the UNCD/substrate interface as the grain colonies coalesce, and thus it is directly related to the nucleation method used.

B. Surface composition and bonding configuration

Motivated by the high quality of the morphology of the UNCD film produced using mechanical polishing with ultrasonic seeding, the surface chemistry and bonding configuration of its topside and underside were examined in further detail by XPS, AES, and XANES.

1. X-ray photoelectron spectroscopy measurements

XPS survey spectra (not shown) taken before the hydrogen plasma treatment reveal oxygen on both the topside and underside of UNCD, with a slightly higher concentration on the underside (~12–15 at. % vs ~8–10 at. % on the topside). A higher resolution C 1*s* spectrum [Fig. 4(a)] on the underside shows the C—C bond peak to be at 284.7 eV, which is indicative of sp^2-hybridized carbon, such as in graphite and amorphous carbon, and is consistent with the C 1*s* XPS measurements reported by McFeely *et al.*[28] However, detecting the state of hybridization quantitatively using XPS is a controversial issue, and there are a number of papers debating this issue. For example, Pate[29] observed the

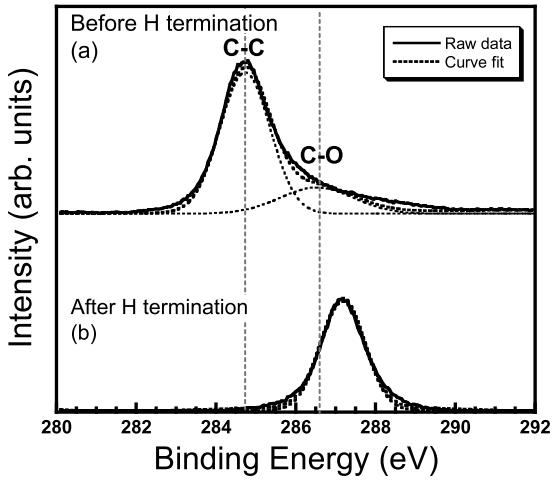

FIG. 4. C 1*s* XPS spectra of the UNCD film from (a) the as-etched underside and (b) the underside surfaces after H termination.

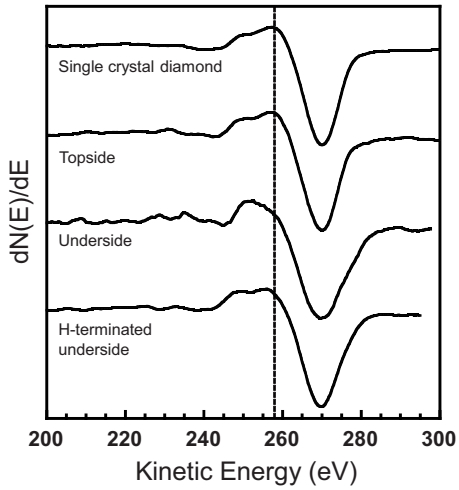

FIG. 5. Auger C *KLL* fine structure obtained on the reference sample single crystal diamond, UNCD topside, as-etched underside, and underside surfaces after H termination, respectively.

same binding energy (284.7 eV) for diamond as well as graphite. Belton and Schmieg[30] had measured 284.75 eV for both diamond and graphite and concluded that pure carbon species have the same binding energy regardless of their hybridization and speculated that measured values may vary from system to system depending on calibration and sample preparation. Surface charging can also shift the peak position in XPS. Therefore, in our experiments, we have used XPS only to detect the presence of other species (e.g., O) and whether or not they are chemically bound to the UNCD (e.g., C—O bonding). We instead rely on AES and XANES to detect small changes in the carbon hybridization state.

In Fig. 4(a), there is a small shoulder toward high binding energy at 286.4 eV. This is due to the C—O bond,[31] confirming that the oxygen is chemically bonded to the carbon. This oxygen arises either from ambient exposure or the residual partial pressure of oxygen in the UNCD growth chamber. The oxygen concentration on the underside may be further affected by the seeding process, the silicon oxide substrate, or the $HF:HNO_3$ etchant used.

After the H-plasma treatment, the high-resolution XPS C 1*s* scan, Fig. 4(b), shows a single peak at 287 eV. This represents the pure C 1*s* peak for the C—C bond with no indication of a C—O bond, but shifted upward by 3.3 eV from the expected 284.7 eV due to charging of the insulating H-treated UNCD surface. The C 1*s* peak for C—H bonding is known to be at 284.85 eV, close to that of pure carbon (C—C) bonding at 284.7 eV, as reported in a high-resolution photoemission study performed using a surface-sensitive mode with a synchrotron source on a single crystal diamond (111) with and without H termination.[32] The small shift of 0.15 eV in binding energy observed in that work cannot be resolved in our XPS due to the energy spread of our source and detector. In addition, the energy shift due to the surface charging further renders this impossible to resolve. Therefore, we have used other surface-sensitive techniques to confirm the presence of H termination, as explained below. A small amount of oxygen (9 at. %) is observed in the XPS survey scan (not shown) and is interpreted as physisorbed species from ambient exposure, since no C—O peak is detected. The XPS data thus confirm that the acid-etched underside of the UNCD surface contains chemisorbed oxygen and possibly amorphous carbon, while the H treatment removes the chemisorbed oxygen and leaves the surface in a more insulating state. The observed charging is consistent with reduced conductivity of the surface due to the removal of any sp^2-bonded carbon and the exclusive presence of diamond-bonded carbon. This observation is more convincingly confirmed by AES and XANES measurements described next.

2. Auger electron spectroscopy measurements

The analysis presented above leads to the conclusion that the use of XPS alone is not sufficient for detecting subtle variations in the hybridization state on UNCD surfaces. While this problem has been discussed in the literature before, some researchers persist in attempting to use XPS to draw conclusions about the hybridization state of carbon surfaces. Additionally, charging of the sample can cause an additional shift and adds further ambiguity in interpreting XPS measurements in terms of hybridization. Lurie and Wilson[33] had shown that it is possible to identify at least three types of carbon phases, namely, diamond, graphite, and amorphous carbon, by examining the AES fine structure of the C *KLL* peak, and they had found that the structure is not significantly affected by charging. The fine structure has been explained based on a band structure model correlating the experimental peaks with the calculated density of states in the respective band structures. The detailed calculations were presented by Painter *et al.*[34] However, fully quantitative, unambiguous interpretation is not yet established. However, it is possible to make qualitative arguments based on specific shapes for the corresponding carbon phases. Figure 5 show AES spectra taken at the C *KLL* edge on a H-terminated single crystal diamond, the UNCD topside, the as-etched underside, and the H-terminated underside, respectively. The topside and the H-terminated underside surfaces show the typical signature corresponding to the diamond phase,

whereas the as-etched underside shows a signature that trends toward that of amorphous carbon, indicating that amorphous carbon is a significant component of the etched underside. The most noticeable feature whose intensity changes due to hybridization is highlighted by the vertical dashed line in Fig. 5. The AES fine structure signatures are consistent with other studies.[33,35] This confirms the presence of some amount of amorphous carbon on the as-etched underside of the UNCD. It further demonstrates that the amorphous carbon phase is selectively etched by the H-plasma treatment, as expected. While the changes observed by AES are reproducible, they are indeed somewhat subtle. More definitive characterization of changes in the hybridization state of carbon is provided by using XANES spectroscopy, as discussed in the next section.

3. X-ray absorption near-edge structure spectroscopy

In XANES spectroscopy,[36] incident x rays excite a core electron to an unoccupied state. The resulting core hole is filled by an electron from a higher shell whose deexcitation leads to the emission of a fluorescence photon (fluorescence yield) or an Auger electron which is inelastically scattered and generates secondary electrons. The secondary electrons dominate the total electron yield (TEY) intensity and emerge from an average sampling depth of ~3 nm for the C *K* edge.[37] Because of the strong dependence of the density of unoccupied states on the local environment, XANES is particularly useful for probing changes in hybridization in carbon-based materials, as well as other chemical bonding states. Unlike Raman spectroscopy, it is equally sensitive to sp^3- and sp^2-bonded carbon as well as other bonding forms.

Figure 6 shows a series of TEY C 1*s* XANES spectra for a reference single crystal diamond sample, the UNCD topside, UNCD underside as-etched, and finally the UNCD underside after H termination. The TEY reference spectrum from the single crystal diamond exhibits distinct and well-established spectral features associated with crystalline sp^3 bonding including the diamond exciton at 289.3 eV and the C $1s \rightarrow \sigma^*$ transitions starting at 289.5 eV which include the second band gap of diamond that produces a pronounced dip at ~302 eV. A small peak associated with sp^2 bonding at 285 eV is due to the C $1s \rightarrow \pi^*$ transition and is ascribed to adventitious carbon adsorbed from the ambient environment as well to π-bonded reconstructed species which may exist at defects, steps, or unsaturated regions on the diamond surface.[38]

The next spectrum in the series shows the C 1*s* XANES spectrum for the topside of the UNCD. The spectrum clearly resolves the sharp absorption edge at 289.5 eV and all expected features above it. The diamond exciton peak at 289.3 eV is slightly broader and somewhat diminished in intensity than that for single crystal diamond, consistent with previous work. This is due to the confinement of the exciton in the nanocrystalline grains.[39] The small peak due to the C $1s \rightarrow \pi^*$ resonance at 285 eV is again due to sp^2-bonded carbon. The sp^2 fraction is calculated to be ~3%, which is slightly lower than the ~5% sp^2 content identified in previous XANES studies[39] due to the grain boundaries of UNCD. This unambiguously demonstrates crystalline sp^3-bonded carbon as the dominant phase in the near-surface region of the topside and is consistent with the most recent XANES studies on UNCD.[12]

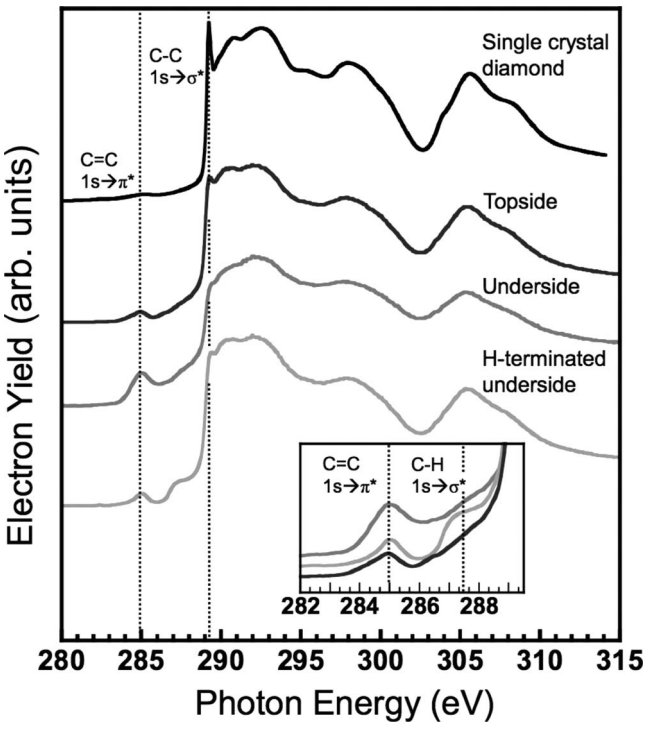

FIG. 6. (a) C 1*s* TEY XANES spectra of the UNCD taken on topside, as-etched underside, and underside surfaces after the hydrogen plasma treatment. The inset shows magnified view of the pre-edge features in the spectra.

The XANES spectrum from the underside of UNCD before exposure to the H plasma is shown next. In comparison to the topside, this spectrum show a more intense C $1s \rightarrow \pi^*$ resonance peak, a less distinct diamond exciton feature, a shallower second band gap dip at 302 eV, and an overall lower yield. The pre-edge features near 285 eV are illustrated in the inset. The sp^2 fraction was found to be ~7%. This demonstrates an increased presence of amorphous carbon. This presence of nondiamond phases is consistent with the AES studies (Fig. 5) and is also consistent with previous cross-sectional TEM studies on a different set of UNCD films, but grown under similar conditions.[3,13] Further analysis reveals enhanced intensity at ~288.5 eV that is ascribed to the C $1s \rightarrow \pi^*$ transition of the C=O bond in carboxyl groups.[36] This is consistent with our XPS measurement shown in Fig. 4(b) where the presence of chemisorbed oxygen is more readily apparent. The amount of sp^2-bonded carbon present on the underside is significantly less than that of the underside of samples seeded by ultrasonic seeding only.[12] The mechanism of formation of the amorphous carbon at the interface is likely due to the induction period before the growing diamond film coalesces and will be discussed in a future publication.

Collectively, the XPS, AES, AFM, and XANES results show unequivocally that the quality of the underside (smoothness, uniformity, absence of voids and/or crevices, and diamond bonding character) is significantly better for the

sample seeded by the method discussed here. Clearly, the quality of the film at the underside is directly related to the seeding process used.

The TEY XANES spectrum from the underside of the UNCD surface after the H-plasma treatment shows a substantial reduction in the C $1s \rightarrow \pi^*$ peak at 285.0 eV, an increase in the sharpness of the exciton feature and the absorption edge at 289.5 eV, and a lower sp^2 fraction (3%) demonstrating a reduction of amorphous carbon and an increase in local diamond character of the near-surface region.

A careful examination of the pre-edge region (Fig. 6, inset) shows a definitive peak at 287.5 eV. This is due to the $1s \rightarrow \sigma^*$ resonance of the C—H bond. There is no shoulder due to the C—O peak feature at 288.5 eV, which is consistent with the XPS measurement [Fig. 4(a)] demonstrating the removal of chemically bonded oxygen from the surface. The H termination of the UNCD surface is further supported by sum frequency generation (SFG) measurements performed separately on a similar UNCD sample (not shown here). The SFG technique has been successfully used before by other groups to show H termination on a single crystal diamond surface.[40]

These results demonstrate that with H-plasma treatment of the UNCD underside, it is possible to obtain a pristine UNCD surface, which is chemically identical to that of the topside. The H-plasma treatment preferentially removes oxidized and amorphous carbon and leaves the diamond surface hydrogen terminated. The final morphology of the underside is extremely smooth and free of crevices, seen in previous studies of films seeded differently. Such crevices are a significant concern for applications such as MEMS/NEMS devices, as they may disrupt the mechanical integrity of the film by providing nucleation sites for crack propagation and fatigue.[14] Roughness may also contribute to enhanced mechanical energy dissipation. The ideal underside of a diamond film, namely, a smooth surface with fully sp^3-bonded grains, can indeed be achieved by the method shown here, which maximizes the initial nucleation density of the film.

4. Nanotribology measurements with atomic force microscopy

To investigate the nanotribological properties of UNCD surfaces, we used AFM to study interfacial adhesion and friction between commercial diamond-coated AFM tips and the UNCD surfaces in ambient air before and after the H-plasma treatment, for both the topside and underside. AFM is used to determine the true work of adhesion between two surfaces by using elastic adhesive single asperity contact mechanics.[41] Two sets of measurements using microcrystalline diamond-coated Si tips (Nanosensors, Phoenix, AZ) were obtained. These measurements, using two separate AFM probes to test for reproducibility, agreed closely. It would, in fact, be preferable to use a UNCD tip, so as to have a self-mated interface. Unfortunately, such tips were not available commercially at the time of this study, but recent progress in our laboratories has demonstrated that it is possible to fabricate monolithic UNCD cantilevers, and commercial availability of such probes has emerged during the revision of this paper. The details of fabricating such probes will be discussed in a future publication.

For analyzing adhesion, the interface is considered to possess an energy per unit area $\gamma = \gamma_1 + \gamma_2 - \gamma_{12}$, where γ_1 and γ_2 are the tip and sample surface energies and γ_{12} the interfacial energy.[42] γ is the Dupré energy or work of adhesion, i.e., the work per unit area required to separate the surfaces from contact to infinity. γ encompasses all interfacial forces and can be used to then predict the force of adhesion in multiasperity interfaces[43] such as those in MEMS devices when the roughness of the surfaces is also taken into account.[44,45] For an elastic, paraboloidal tip in contact with a flat, homogeneous, isotropic, linear elastic surface, the adhesion behavior spans a spectrum from the Johnson-Kendall-Roberts (JKR) model[46] (for large tips and compliant materials with strong, short-range adhesion) to the Derjaguin-Müller-Toporov (DMT) model[47] (for small tips and stiff materials with weak, long-range adhesion). γ is determined from the force F_{PO} required to pull the tip out of contact with the surface:

$$\gamma = \frac{-F_{PO}}{\chi \pi R},$$

where χ ranges monotonically from 1.5 (JKR) to 2 (DMT). Tabor's parameter μ_T can be used to select the value between these two limits that applies:[41,48]

$$\mu_T = \left(\frac{16R\gamma^2}{9K^2 z_0^3}\right)^{1/3} = \left(\frac{16F_{PO}^2}{9\chi^2\pi^2 RK^2 z_0^3}\right)^{1/3},$$

where R is the tip radius and K is the contact modulus, given by $K = (4/3)[(1-\nu_1^2)/E_1 + (1-\nu_2^2)/E_2]^{-1}$. E_1 and E_2 are the Young's moduli, and ν_1 and ν_2 are the Poisson's ratios of the tip and sample, respectively. The parameter z_0 is the equilibrium separation of the surfaces in contact and is assumed to represent the length scale of the interfacial forces. $\mu_T > 5$ ($\mu_T < 0.1$) implies the JKR (DMT) limit. Unfortunately, neither z_0 nor χ are not known *a priori*. However, following the methodology described previously,[49] an upper bound estimate of μ_T is made by assuming the smallest reasonable value for z_0 of 0.154 nm, which is the C—C bond distance in diamond. Since the AFM tips were coated with a diamond film, we use a tip modulus of 1.16 TPa and take Poisson's ratio for the tip to be that of diamond, $\nu_1 = 0.08$, corresponding to the diamond (111) plane.[50] Young's modulus and Poisson's ratio for UNCD were taken to be 960 GPa (Ref. 10) and 0.07,[50] respectively. The tip shape and radius were measured using TEM imaging (Fig. 7, insets). The roughness of the microcrystalline diamond tip coating is apparent and is clearly not ideal for these measurements. However, fitting a paraboloidal shape to the tip profile with a radius of 78 nm provides a reasonable estimate. TEM images are taken before and after the measurements and show no observable modification to the tip [Fig. 7(b)]. We then used the smallest possible value of $\chi = 1.5$ and solved for the largest possible value of μ_T using the average value of the measured pull-off force F_{PO}. To reduce the possibility of tip wear, F_{PO} was measured without any in-plane scanning. F_{PO} was measured on several locations of the sample at least 35 times per tip. Choosing the cases that exhibited the larger values of F_{PO},

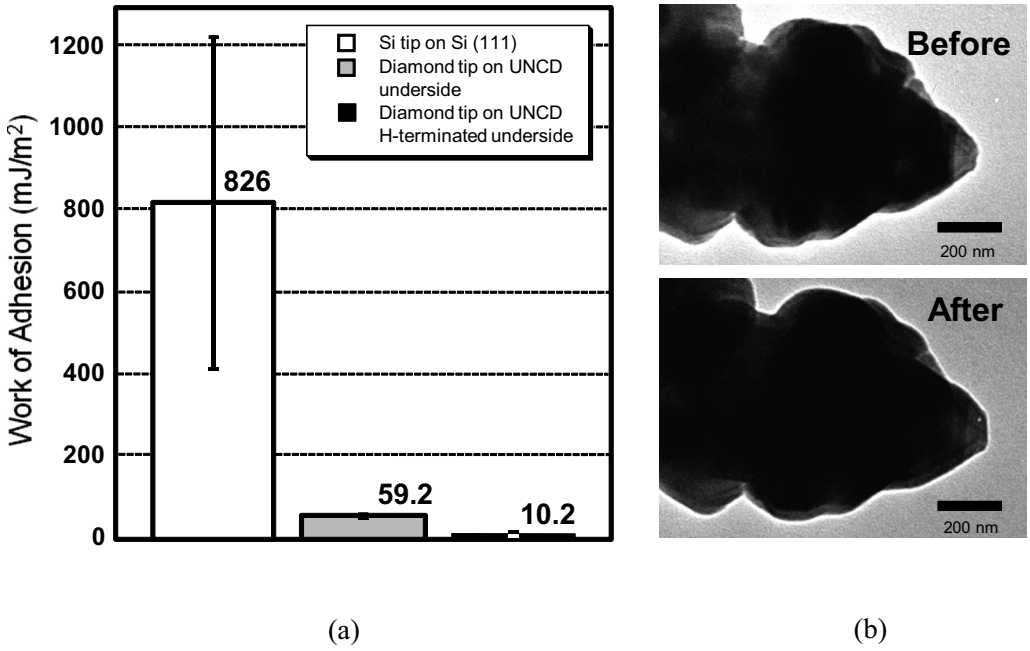

FIG. 7. (a) Work of adhesion between a diamond-coated tip and UNCD underside surfaces before and after H termination. Results for a silicon tip making contact with a single crystal silicon (111) wafer (both the tip and sample have a native oxide) are included for comparison. (b) TEM images of the diamond-coated tip used for adhesion measurements, demonstrating no measurable change after the measurements.

we find that Tabor's parameter does not exceed 0.13. Since this value was calculated using the most extreme assumptions, we conclude that the interface is firmly in the DMT regime, i.e., $\chi=2$, and γ can now be determined from the pull-off force. We used a model intermediate to the JKR and DMT regimes[45,48] to calculate the work of adhesion for the silicon sample using a silicon AFM tip.

The work of adhesion values is plotted in Fig. 7(a). Results for a silicon tip making contact with a single crystal silicon (111) wafer are included for comparison. Both the tip and sample have a naturally hydrophilic native oxide. The Si surface was cleaned using First Contact, a contamination removal polymer film (Photonic Cleaning Technologies, Platteville, WI). This cleaning procedure leaves the surface free of debris and contamination according to optical microscopy and AFM topographic imaging. Any substrate exposed to air will possess both water and adventitious hydrocarbon contamination. Thus, as with any other AFM measurement in air, the precise surface chemistry is unknown. The details of the Si-on-Si measurements are described elsewhere.[51]

Si-on-Si shows the highest value and statistical scatter for the work of adhesion, 826 ± 186 mJ/m^2. The high surface energy of the hydrophilic native oxide leads to the high work of adhesion. Capillary condensation from the ambient environment may also contribute. Variations in surface contamination and water condensation may account for the high variability in the measurements, which leads to the large statistical error reported. The diamond-UNCD underside interface, before H exposure, exhibits a substantially lower work of adhesion, 59.2 ± 2 mJ/m^2, than Si-on-Si. The H-plasma treatment of the underside reduced the work of adhesion with the diamond tip significantly to 10.2 ± 0.4 mJ/m^2. This value is very low in an absolute sense: It is lower than that found for inert, saturated hydrocarbon interfaces[42] which are in the range of 25–35 mJ/m^2. In these systems, adhesion is entirely due to van der Waals' interactions. This indicates that all other interfacial adhesion mechanisms such as covalent bonding, surface charge and dipole interactions, and meniscus formation have been eliminated. We have reduced adhesion to the range of van der Waals' interactions. Enachescu *et al.*[52] measured a work of adhesion of ~10 mJ/m^2 for an oxidized tungsten carbide AFM tip on H-terminated single crystal diamond (111) in ultrahigh vacuum. However, their cantilever was not experimentally calibrated, unlike the method used here, and is therefore subject to significant uncertainty. We previously measured adhesion between a tungsten carbide tip and single crystal diamond (111) as well as the UNCD underside (as etched and after H termination) in air and found that after H termination, the work of adhesion on the UNCD underside was in the range of 32–36 mJ/m^2, as compared to 40–45 mJ/m^2 measured on the H-terminated single crystal diamond.[12] A recent *ab initio* calculation using density functional theory (DFT) found that the work of adhesion was 8 mJ/m^2 for two H-terminated C(111) single crystal surfaces in contact.[53] The DFT calculation does not include van der Waals' interactions. Thus, the value obtained represents contributions from small, nonbonded electrostatic effects. The fact that these other interactions are not predicted to be larger than our result demonstrates that our measurements are physically reasonable.

We also measured friction between the diamond-coated tips and UNCD underside before and after the H-plasma treatment [Fig. 8(a)]. Friction is measured at a zero externally applied load (i.e., only adhesion is holding the tip onto the surface). The force of friction is reduced significantly by

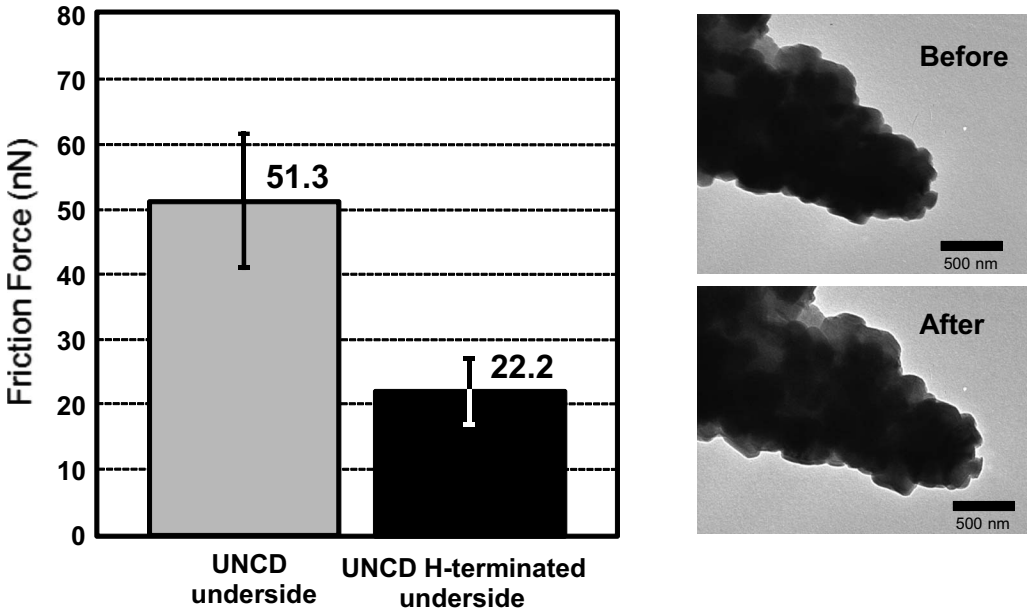

(a) (b)

FIG. 8. (a) Nanoscale friction force experienced by a diamond-coated tip scanning against the UNCD underside surface before and after H termination, measured at zero externally applied load. (b) TEM images of the diamond-coated tip used for this experiment, demonstrating no measurable wear.

the H-plasma treatment, from 51.3±10.3 to 22.2±5.1 nN. The significant statistical errors in both the adhesion and friction data are not surprising since the actual contact area is only a few nanometers, so small variations in sample morphology and surface composition can alter individual measurements. Friction measurements on Si were avoided because sliding-induced contamination of tips rendered measurements irreproducible. TEM characterization of the tip radius before and after friction measurements [Fig. 8(b)] did not show any measurable change in the tip radius.

The reduction in friction by H termination of diamond is consistent with molecular dynamics simulations studies by Gao *et al.*[54] in which friction was studied as function of load at the interface between a diamond (111) surface and an amorphous carbon film. The diamond counterface was terminated with varying percentages of hydrogen coverage (80%–100%). It was found that friction forces were reduced at all loads for increased levels of hydrogen coverage.

We conclude that H termination removes contaminants including polar oxide groups, saturates dangling bonds, and leaves an inert surface that has both lower adhesion and a lower resistance to sliding leading to much lower adhesion and friction at higher H coverage. A more detailed study of friction as a function of load on UNCD surfaces is in progress and will be presented separately.

IV. CONCLUSIONS

The characterization of the surface chemistry and hybridization state of carbon in nanostructured carbon-based materials is of increasing technological and scientific interest, as they have a strong effect on the nanoscale mechanical, chemical, and tribological properties. To determine the hybridization state of carbon, the synchrotron-based XANES technique is critical in providing definitive, surface-sensitive measurements as it provides the most distinct fingerprints for the different hybridization states of carbon. AES does offer the advantage of being a simpler, faster, semiquantitative, surface-sensitive method of characterizing carbon-based films. Our results show that this widely available method does provide a degree of useful and rapid characterization when a synchrotron source is not readily accessible. XPS, on the other hands, suffers from being the most insensitive method for characterizing the hybridization state of carbon. It is, of course, effective at detecting the presence and chemical bonding state of contaminant species such as oxygen. While this latter point has been appreciated as one of the most basic capabilities of XPS, the former point remains somewhat poorly understood and inconsistently applied in the literature.

By applying a combination of SEM, AFM, XPS, AES, and XANES, we can make definitive conclusions about the surface chemistry and bonding configuration of UNCD surfaces and how the nanotribological properties are subsequently affected. By etching away the substrate, we find that the seeding process significantly affects the surface morphology and phase of the underside of UNCD films. High nucleation density is essential for reducing the initial presence of nondiamond phases and ensuring a smooth surface morphology. Generally, the acid-etched underside surface is overwhelmingly sp^3-bonded, but with a higher fraction of nondiamond phases (amorphous carbon and some oxidized carbon) than the as-grown topside. Adhesion between the

as-etched underside and a diamond tip is lower by a factor of ~14 compared to a Si—Si interface. The surface chemistry and bonding configuration of the underside can be further improved by using a H-plasma treatment. However, if the film was poorly nucleated, then crevices will be created on the underside.[11] This morphology will be unfavorable for mechanical device applications that demand a uniform, smooth morphology. Regardless of the morphology, the remaining exposed material is now purely hydrogen-terminated UNCD. This minimizes nanoscale adhesion to near the van der Waals' limit (~80 times less than for a Si—Si interface) and reduces friction correspondingly. A remaining issue is the extent to which the highly confined underside of MEMS/NEMS structural layers (usually separated from other layers only by a submicron gap) can be treated by a hydrogen plasma.

Our methodology, of characterizing and tailoring surfaces that will be relevant for tribological situations, not only applies to UNCD films but is also relevant to other thin film materials including silicon, silicon carbide, and others being explored as alternatives for MEMS/NEMS devices. Given the critical role that surface forces play, this study provides a general methodology for characterizing and optimizing surfaces for tribological applications including those in MEMS/NEMS devices.

ACKNOWLEDGMENTS

This work was supported by the Air Force Office of Scientific Research under Contract No. FA9550-05-1-0204 and the U.S. Department of Energy, BES-Materials Sciences, under Contracts No. DE-FG02-02ER46016 and No. W-13-109-ENG-38. Use of the Center for Nanoscale Materials was supported by the U. S. Department of Energy, Office of Science, Office of Basic Energy Sciences, under Contract No. DE-AC02-06CH11357. The authors gratefully acknowledge R. J. Hamers and Wensha Yang for their help in using their rf-plasma setup for hydrogen termination experiments. The authors thank E. E. Flater for the Si—Si adhesion measurements and R. J. Cannara for providing AES reference spectra taken on single crystal diamond. The authors acknowledge J. Denlinger for his help on the SXF spectrometer at ALS. The XANES measurements were performed at the Advanced Light Source and are supported by Director, Office of Science, Office of Basic Energy Science, Materials Sciences Division of the U.S. Department of Energy under Contract No. DE-AC03-76SF00098 at Lawrence Berkeley National Laboratory.

*Present address: Center for Nanoscale Materials, Argonne National Laboratory, Argonne, IL.
†Present address: Dow Chemical Company, Midland, MI.
‡Present address: Advanced Diamond Technologies, Inc, Romeoville, IL.
§Present address: Department of Mechanical Engineering and Applied Mechanics, University of Pennsylvania, Philadelphia, PA.

[1] R. F. Davis, in *Diamond Films and Coatings*, edited by R. F. Davis (Noyes, Park Ridge, NJ, 1992).
[2] J. Philip, P. Hess, T. Feygelson, J. E. Butler, S. Chattopadhyay, K. H. Chen, and L. C. Chen, J. Appl. Phys. **93**, 2164 (2003).
[3] D. M. Gruen, Annu. Rev. Mater. Sci. **29**, 211 (1999).
[4] K. C. Holmes, J. L. Davidson, W. P. Kang, and A. L. Stemberg, *2001 Microelectromechanical Systems Conference, Berkeley, CA* (IEEE Xplore, 2001), p. 45.
[5] L. Sekaric, J. M. Parpia, H. G. Craighead, T. Feygelson, B. H. Houston, and J. E. Butler, Appl. Phys. Lett. **81**, 4455 (2002).
[6] E. Kohn, W. Ebert, M. Adamschik, P. Schmid, and A. Denisenko, New Diamond Front. Carbon Technol. **11**, 81 (2001).
[7] J. L. Davidson, W. P. Kang, Y. Gurbuz, K. C. Holmes, L. G. Davis, A. Wisitsora-at, D. V. Kerns, R. L. Eidson, and T. Henderson, Diamond Relat. Mater. **8**, 1741 (1999).
[8] O. Auciello, J. Birrell, J. A. Carlisle, J. E. Gerbi, X. Xiao, B. Peng, and H. D. Espinosa, J. Phys.: Condens. Matter **16**, 539 (2004).
[9] A. V. Sumant, O. Auciello, A. R. Krauss, D. M. Gruen, D. Ersoy, J. Tucek, A. Jayatissa, E. Stach, N. Moldovan, D. Mancini, H. G. Busmann, and E. M. Meyer, in *Materials Science of Microelectromechamical Systems (MEMS) Devices III*, edited by M. deBoer, M. Judy, H. Kahn, and S. M. Spearing, MRS Symposia Proceedings No. 657 (Materials Research Society, Pittsburgh, 2001), p. 5.
[10] H. D. Espinosa, B. C. Prorok, B. Peng, K. H. Kim, N. Moldovan, O. Auciello, J. A. Carlisle, D. M. Gruen, and D. C. Mancini, Exp. Mech. **43**, 256 (2003).
[11] H. D. Espinosa and B. Peng, J. Microelectromech. Syst. **14**, 153 (2005).
[12] A. V. Sumant, D. S. Grierson, J. E. Gerbi, J. Birrell, U. D. Lanke, O. Auciello, J. A. Carlisle, and R. W. Carpick, Adv. Mater. **17**, 1039 (2005).
[13] S. Jiao, A. Sumant, M. A. Kirk, D. M. Gruen, A. R. Krauss, and O. Auciello, J. Appl. Phys. **90**, 118 (2001).
[14] H. D. Espinosa, B. Peng, B. C. Prorok, N. Moldovan, O. Auciello, J. A. Carlisle, D. M. Gruen, and D. C. Mancini, J. Appl. Phys. **94**, 6076 (2003).
[15] A. V. Sumant, P. U. P. A. Gilbert, D. S. Grierson, A. R. Konicek, M. Abrecht, J. E. Butler, T. Feygelson, S. S. Rotter, and R. W. Carpick, Diamond Relat. Mater. **16**, 718 (2007).
[16] J. E. Sader, J. W. M. Chon, and P. Mulvaney, Rev. Sci. Instrum. **70**, 3967 (1999).
[17] D. F. Ogletree, R. W. Carpick, and M. Salmeron, Rev. Sci. Instrum. **67**, 3298 (1996).
[18] J. C. Arnault, L. Demuynck, C. Speisser, and F. Le Normand, Eur. Phys. J. B **11**, 327 (1999).
[19] K. F. Turner, Y. M. LeGrice, B. R. Stoner, J. T. Glass, and R. J. Nemanich, J. Vac. Sci. Technol. B **9**, 914 (1991).
[20] E. Anger, A. Gicquel, Z. Z. Wang, and M. F. Ravet, Diamond Relat. Mater. **4**, 759 (1995).
[21] Y. Chakk, R. Brener, and A. Hoffman, Appl. Phys. Lett. **66**, 2819 (1995).
[22] S. Lijima, Y. Aikawa, and K. Baba, Appl. Phys. Lett. **57**, 2646 (1990).

[23] H.-W. Ko, C. K. Chen, and C.-H. J. Liu, Diamond Relat. Mater. **5**, 861 (1996).
[24] S. Pecoraro, J. C. Arnault, and J. Werckmann, Diamond Relat. Mater. **14**, 137 (2005).
[25] S. Rotter, in *Proceedings of the Applied Diamond Conference/ Frontier Carbon Technologies-ADC/FCT'99*, edited by M. Yoshikawa, Y. Koga, Y. Tzeng, C. P. Klages, and K. Miyoshi (MYU K. K., Tokyo, 1999), p. 25.
[26] T. H. Metcalf, X. Liu, B. H. Houston, J. W. Baldwin, J. E. Butler, and T. Feygelson, Appl. Phys. Lett. **86**, 081910 (2005).
[27] T. R. Anthony, Vacuum **41**, 1356 (1990).
[28] F. R. McFeely, S. P. Kowalezyk, L. Ley, R. G. Cavell, R. A. Pollak, and D. A. Shirley, Phys. Rev. B **9**, 5268 (1974).
[29] B. B. Pate, Surf. Sci. **165**, 83 (1986).
[30] D. N. Belton and S. J. Schmieg, J. Vac. Sci. Technol. A **8**, 2353 (1990).
[31] D. H. C. Chua, W. I. Milne, D. Sheeja, B. K. Tay, and D. Schneider, J. Vac. Sci. Technol. B **22**, 2680 (2004).
[32] J. F. Morar, F. J. Himpsel, G. Hollinger, J. L. Jordan, G. Hughes, and F. R. McFeely, Phys. Rev. B **33**, 1340 (1986).
[33] P. G. Lurie and J. M. Wilson, Surf. Sci. **65**, 476 (1977).
[34] G. S. Painter, D. E. Ellis, and A. R. Lubinsky, Phys. Rev. B **4**, 3610 (1971).
[35] B. E. Williams and J. T. Glass, J. Mater. Res. **4**, 373 (1989).
[36] J. Stöhr, *NEXAFS Spectroscopy* (Springer-Verlag, Berlin, 1992).
[37] B. H. Frazer, B. Gilbert, B. R. Sonderegger, and G. De Stasio, Surf. Sci. **537**, 161 (2003).
[38] R. Graupner, J. Ristein, L. Ley, and C. Jung, Phys. Rev. B **60**, 17023 (1999).
[39] J. Birrell, J. E. Gerbi, J. A. Carlisle, O. Auciello, D. M. Gruen, and J. M. Gibson, J. Appl. Phys. **93**, 5606 (2003).
[40] R. P. Chin, J. Y. Huang, Y. R. Shen, T. J. Chuang, and H. Seki, Phys. Rev. B **52**, 5985 (1995).
[41] K. Johnson and J. Greenwood, J. Colloid Interface Sci. **192**, 326 (1997).
[42] J. N. Israelachvili, *Intermolecular and Surface Forces* (Academic, London, 1992).
[43] D. Maugis, J. Adhes. Sci. Technol. **10**, 161 (1996).
[44] K. Komvopoulos and W. Yan,Trans. ASME, J. Tribol. **119**, 391 (1997).
[45] M. P. de Boer and T. A. Michalske, J. Appl. Phys. **86**, 817 (1999).
[46] K. L. Johnson, K. Kendall, and A. D. Roberts, Proc. R. Soc. London, Ser. A **324**, 301 (1971).
[47] B. V. Derjaguin, V. M. Müller, and Y. P. Toporov, J. Colloid Interface Sci. **53**, 314 (1975).
[48] D. Tabor, J. Colloid Interface Sci. **58**, 2 (1977).
[49] D. S. Grierson, E. E. Flater, and R. W. Carpick, J. Adhes. Sci. Technol. **19**, 291 (2005).
[50] C. A. Klein, Mater. Res. Bull. **27**, 1407 (1992).
[51] E. E. Flater, W. R. Ashurst, and R. W. Carpick, Langmuir **23**, 9242 (2007).
[52] M. Enachescu, R. J. A. van den Oetelaar, R. W. Carpick, D. F. Ogletree, C. F. J. Flipse, and M. Salmeron, Phys. Rev. Lett. **81**, 1877 (1998).
[53] Y. Qi, E. Konca, and A. T. Alpas, Surf. Sci. **600**, 2955 (2006).
[54] G. T. Gao, P. T. Mikulski, and J. A. Harrison, J. Am. Chem. Soc. **124**, 7202 (2002).